A Model of the Interdiffused Multilayer Process

SPYROS A. SVORONOS and WILBUR W. WOO

University of Florida, Department of Chemical Engineering, Gainesville, FL 32611

STUART J.C. IRVINE

Multidisciplinary Research and Innovation Centre, North East Wales Institute, Plas Coch, Mold Road, Wrexham, Clwyd LL11 2AW, United Kingdom

HALUK O. SANKUR and JAGMOHAN BAJAJ

Rockwell International Corporation, Science Center, 1049 Camino Dos Rios, Thousand Oaks, CA 91360

The interdiffused multilayer process (IMP) is a novel approach to growing $Hg_{1-x}Cd_xTe$. In this process, alternating thin films of HgTe and CdTe are grown and allowed to interdiffuse resulting in a bulk material of constant composition. A model of the IMP must include the effects of both the deposition of new material and the interdiffusion of the material. It must also be able handle the flush phases of the IMP where the growth rate decays to zero. Existing approaches to modeling epitaxial growth of $Hg_{1-x}Cd_xTe$ treat growth and interdiffusion as separate, sequential steps resulting in numerical stability problems, pseudodiffusion effects, or flush phase modeling problems. The model presented here, however, is based on an incremental balance where growth and diffusion occur simultaneously, resulting in a model exhibiting none of the difficulties mentioned above. The IMP growth model is integrated with a model for calculating reflectance from a laser directed at near normal incidence angle. The predicted reflectance is compared to experimental measurements and showed a good preliminary fit when the model employed default parameters. The agreement is greatly improved after parameter fitting.

Key words: HgCdTe, in situ monitoring, interdiffused multilayer process, laser reflectance, MOCVD, modeling

INTRODUCTION

The II-VI ternary compound semiconductor mercury cadmium telluride (MCT), $Hg_{1-x}Cd_xTe$, is used in the fabrication of infrared detectors and focal plane arrays because the bandgap energy, and therefore the optical responsivity, can easily be adjusted by changing the group II Cd mole fraction x. The interdiffused multilayer process[1–4] (IMP) is a novel approach for growing uniform layers of MCT at any desired x. In this process, metalorganic chemical vapor deposition (MOCVD) is used to grow alternating very thin (≤0.2 μm thick) layers of HgTe and CdTe. These layers interdiffuse during the growth and subsequent annealing period resulting in a film of MCT of uniform composition. By adjusting the relative thicknesses of the HgTe and CdTe layers, any desired x can be achieved. An important advantage of the IMP is that it allows individual optimization of the HgTe and CdTe growth phases.

(Received December 1, 1995; revised March 1, 1996)

In this paper, a model of the growth and interdiffusion processes on the IMP is presented. The model takes into account deposition of new material on top of the wafer and interdiffusion between the CdTe and HgTe layers. This model is then integrated with a normal incidence laser reflectance model and tested against in situ IMP reflectance measurements.

MODELING OF FILM GROWTH AND INTERDIFFUSION

A mathematical model of the IMP must account for deposition at the top of the wafer and for HgTe/CdTe

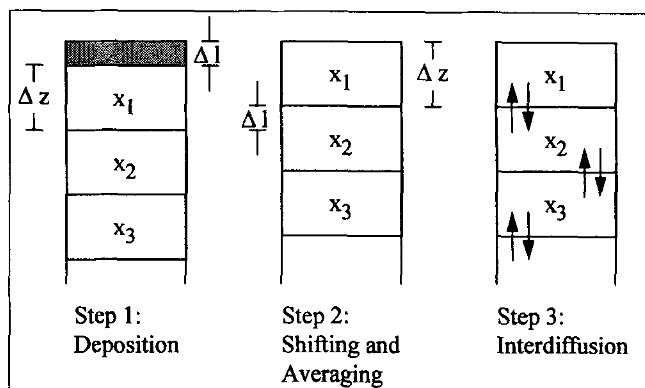

Fig. 1. Integration iterative steps if deposition and diffusion are treated as separate sequential steps.

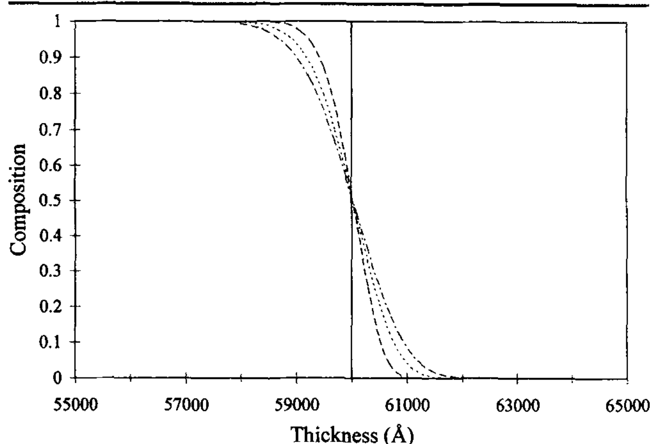

Fig. 2. Composition profile as a function of time for a deposition rate 10Å/s and D = 0 with increments $\Delta t = 1$ s and $\Delta z = 200$Å. The interface is at 60000Å. The solid line shows the correct profile for all t. The dashed line is at t = 100 s, the dotted line at t = 200 s, and the dashed-dotted line at t = 300 s.

interdiffusion along the wafer depth. A mass balance at an interior point yields the partial differential equation

$$\frac{\partial x}{\partial t} = \frac{\partial}{\partial z}\left(D\frac{\partial x}{\partial z}\right) \tag{1}$$

Here z denotes the perpendicular distance to the surface, t time, and D is the diffusivity. Before proceeding with discretization of Eq. (1), an expression for D must be obtained.

Diffusivity Expression

Several studies on diffusion in MCT have been published.[5–20] There is a consensus that at high temperatures (400–750°C) HgTe/CdTe interdiffusion is fairly independent of the Hg partial pressure[6–9] while at lower temperatures the effect of Hg partial pressures becomes significant.[6,7,10]

Interdiffusion probably involves both metal vacancies and interstitials with the interstitials becoming increasingly important as the temperature decreases and x increases.[6,11] There is evidence[8] that at about 350°C, the dominant mechanism changes explaining why expressions for diffusivity developed for the high temperature range extrapolate poorly to lower temperatures.

Usually the IMP is run at temperatures close to 400°C. The high temperature diffusivity expressions agree that D exponentially decreases three to four orders of magnitude as x increases from zero to one. Tang and Stevenson[11,12] as well as Zanio and Massopust[13] provide expressions that at constant temperature become

$$D(x) = A \cdot e^{-Bx} \tag{2}$$

Previous Work in Solving the Diffusion Equation for MCT Growth

Finding a solution to the diffusion equation is challenging because of the nonlinear dependence of the diffusivity on x, Eq. (2), and because of the moving boundary due to growth. Because of this, an analytical solution is not possible.

Previous numerical approaches to the problem[13–16] of modeling epitaxial growth of MCT treated the deposition and diffusion processes as separate sequential steps. Let Δt and Δz denote the time and distance increments used in the discretization of Eq. (1), respectively. Then the following iterative steps were used:

1. A new film of thickness $\Delta l = g\,\Delta t$, where g is the growth rate of the new material, is deposited on top of layer 1. This material has a composition of x_d.
2. New layers are created by shifting each of the previous layers upward by Δl. The composition of a new layer is calculated by averaging the layer's pre-shift composition and the pre-shift composition of the layer above it. This average is weighted using the thickness that each of the pre-shift layers contributes to the new layer, i.e.

$$x_{new,i} = \frac{\Delta l}{\Delta z} x_{pre\text{-}shift,\,i-1} + \left(1 - \frac{\Delta l}{\Delta z}\right) x_{pre\text{-}shift,i}$$

3. Composition changes due to interdiffusion in the time Δt are calculated for each layer according to a discretization of Eq. (1).

After completion of step 3, time is increased by Δt and steps 1–3 are repeated. Figure 1 is a schematic of this algorithm.

Zanio and Massopust[13] and Zanio[14] used the above scheme with constant Δt and $\Delta l < \Delta z$. Eq. (1) and Eq. (2) were explicitly discretized. Due to numerical stability considerations, step 3 was divided into n substeps, each of duration $\delta t = \Delta t/n$. For a forward time centered space (FTCS) explicit scheme, numerical stability requires[21]

$$\Delta t \le \left(\frac{\Delta z^2}{2D}\right) \tag{3}$$

If D is given by Eq. (2), in Eq. (3) requires that $\Delta t < 0.08$ s for $\Delta z = 50$Å and $\Delta t < 0.003$ s for $\Delta z = 10$Å.

Step 2 of the above algorithm results in an error that can be significant. The averaging of the compositions involved is equivalent to an infinite diffusivity between the bottom of layer i-1 and the top of layer i. This results in pseudodiffusion, even if the actual diffusivity is zero and can lead to considerable error. For example, if the actual diffusivity were zero and the deposition rate of HgTe on CdTe were g = 10Å/s, increments of $\Delta t = 1$ s and $\Delta z = 200$Å would lead to an erroneous HgTe migration of 2000Å in 300 s. Figure 2 shows the effect of this pseudodiffusion. This error may be reduced by increasing Δt or decreasing Δz but at the cost of possible stability problems by in Eq. (3). Furthermore, increasing Δt decreases the integration accuracy, while decreasing Δz increases the dimensionality, i.e. the number of layers, of the problem. Errors due to averaging can be eliminated if $\Delta l = \Delta z$. However, in Eq. (3) requires

$$\Delta z > \frac{2D}{g} \tag{4}$$

For a typical HgTe growth rate of 15Å/s and D given by Eq. (2) with x = 0 at a temperature of 380°C, Eq. (4) requires $\Delta z > 2000$Å which is thicker than the 300Å CdTe films in the IMP.

To allow usage of $\Delta t = \Delta z/g$ (which eliminates averaging error) for a small Δz an implicit discretization scheme must be used. Since the diffusivity is a nonlinear function of z, Eq. (2) must either be linearized or a set of nonlinear differential equations must be solved at each iteration step. Ludington[15] linearized and used a Crank-Nicholson (Press et al.)[21] numerical integration scheme.

Stability problems, however, prevented usage of a reasonable Δz (~50Å). Rossouw et al.[16] used a different implicit scheme and $\Delta t = \Delta z/g$, and encountered no stability problems with $\Delta z = 50$Å. However, their implicit scheme is of suspect accuracy since the right-hand side of Eq. (1) was discretized using at time t+1 the diffusivity D(x(t)). A fully implicit discretization of Eq. (1) can be obtained by backward differencing the left-hand side, center space differencing the right-hand side, i.e.

$$\frac{x_i(t+1)-x_i(t)}{\Delta t} = \tag{5}$$

$$\frac{1}{\Delta z}\left[D\left(\frac{x_i(t+1)+x_{i+1}(t+1)}{2}\right)\frac{x_{i+1}(t+1)-x_i(t+1)}{\Delta z} - D\left(\frac{x_i(t+1)+x_{i-1}(t+1)}{2}\right)\frac{x_i(t+1)-x_{i-1}(t+1)}{\Delta z}\right]$$

and doing a Taylor series expansion on the right-hand side around t. This results in a tri-diagonal linear system which can be easily solved, and which is stable at $\Delta t = \Delta z/g$ for all Δz tested (down to 10Å).

Unfortunately, the above scheme runs into difficulty when applied to the IMP. Deposition phases are followed by flush phases where diffusion takes place and the growth rate decays toward zero. Thus, using the formula $\Delta t = \Delta z/g$ causes trouble. In conclusion, previous work on solving the differential equations for MCT growth is not suitable for the interdiffused multilayer process.

The New Approach

In reality deposition and diffusion take place simultaneously and not as separate and sequential steps. The partial differential equation for diffusion Eq. (1) can be derived by doing an incremental balance at an interior point with increments Δt and Δz, and subsequently taking their limits to zero. In a sense, discretization of Eq. (1) simply inverts the second part of this process resulting in an incremental balance. Therefore, growth rate and deposition can be modeled simultaneously by doing an incremental balance at the top of the wafer which is the only part directly affected by deposition.

Let layer 1 be the layer on which deposition takes place (Fig. 3). The thickness of layer 1, Δl, is not constant, but increases due to growth. A material balance on CdTe for layer 1 gives:

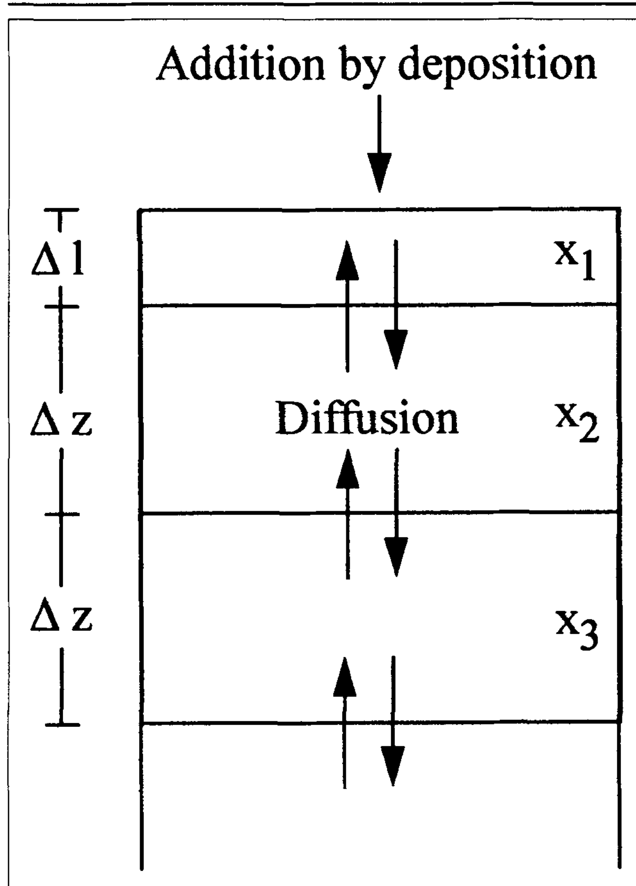

Fig. 3. Top layers of the new algorithm. Δl is the thickness of the top layer (layer 1) with composition x_1. Δz is the thickness of the other layers. Layer 1 has transportation in and out due to new growth and diffusion from layer 2. The remaining layers have transportation due to diffusion from the above and below lying layers.

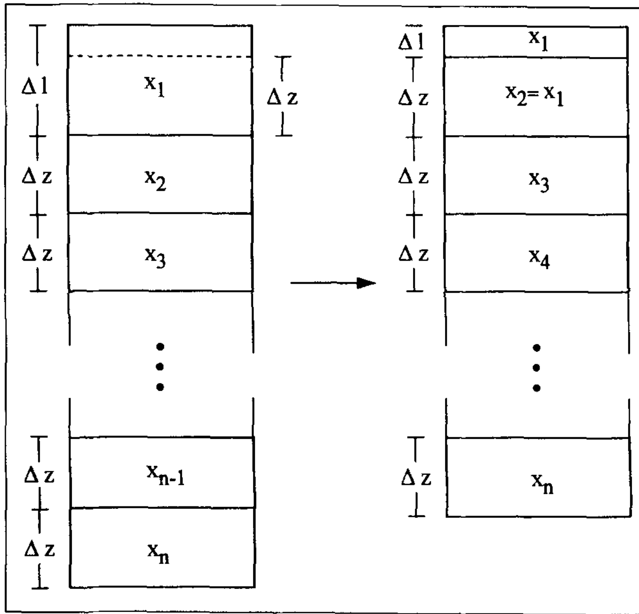

Fig. 4. The shifting scheme of the new algorithm. Whenever Δl surpasses Δz, the top layer is divided into two parts and indices of each of the underlying layers are increased by one. The bottom layer is discarded.

$$\frac{\partial(A\Delta l c x)}{\partial t} = Agcx_d + \left(AD(x)c\frac{\partial x}{\partial z}\right)_{1-2} \tag{6}$$

$$\begin{pmatrix}\text{Accumulation}\\ \text{Rate}\end{pmatrix} = \begin{pmatrix}\text{Addition by}\\ \text{Growth}\end{pmatrix} + \begin{pmatrix}\text{Rate in from layer}\\ \text{2 due to diffusion}\end{pmatrix}$$

where A is the cross-sectional area, c the overall concentration, x_d the deposition mole fraction (0 or 1 in IMP) and $(\,)_{1-2}$ denotes evaluation at the interface between layers 1 and 2. Assuming A and c are constant, they cancel out giving:

$$\frac{\partial(\Delta l x)}{\partial t} = gx_d + \left(D(x)\frac{\partial x}{\partial z}\right)_{1-2} \tag{7}$$

Since the rate of change of Δl is the growth rate,

$$\frac{\partial(\Delta l)}{\partial t} = g \tag{8}$$

and

$$\frac{\partial(\Delta l x)}{\partial t} = \Delta l\frac{\partial x}{\partial t} + gx \tag{9}$$

Substituting Eq. (9) into Eq. (7) gives

$$\frac{\partial x}{\partial t} = \frac{1}{\Delta l}\left[g(x_d - x) + \left(D(x)\frac{\partial x}{\partial z}\right)_{1-2}\right] \tag{10}$$

Taking x at the interface between layers 1 and 2 to be the average of x_1 and x_2 and noting that the distance between the midpoints of the layers is $(\Delta l + \Delta z)/2$, the right-hand side of Eq. (10) is discretized as:

$$\frac{1}{\Delta l}\left[g(x_d - x) + \left(D(x)\frac{\partial x}{\partial z}\right)_{1-2}\right] \cong \tag{11}$$

$$\frac{1}{\Delta l}\left[g(x_d - x) + D\left(\frac{x_1 + x_2}{2}\right)\frac{x_2 - x_1}{\left(\frac{\Delta l + \Delta z}{2}\right)}\right] \equiv Q_1$$

Discretizing the left-hand side of Eq. (10) by either a forward or backward difference gives an explicit or implicit scheme, respectively. These options can be combined into one equation:

$$x_1(t+1) = x_1(t) + \Delta t\left[a_1Q_1(t+1) + (1-a_1)Q_1(t)\right] \tag{12}$$

where $a_1 = 0$ gives an explicit scheme and $a_1 = 1$ gives a fully implicit scheme. Intermediate values of a_1 give combination schemes with $a_1 = 0.5$ giving a Crank-Nicholson analogue.

A similar material balance on layer i where $i \geq 2$ results in

$$\frac{\partial x}{\partial t} = \frac{1}{\Delta z}\left[\left(D(x)\frac{\partial x}{\partial z}\right)_{i-(i+1)} - \left(D(x)\frac{\partial x}{\partial z}\right)_{(i-1)-i}\right] \tag{13}$$

which in the limit that $\Delta z \to 0$ yields the diffusion equation Eq. (1). Proceeding to discretize Eq. (13) in a manner analogous to the discretization of Eq. (10) gives

$$x_1(t+1) = x_1(t) + \Delta t\left[a_1Q_i(t+1) + (1-a_1)Q_i(t)\right] \tag{14}$$

where

$$Q_2 = \frac{1}{\Delta z}\left[D\left(\frac{x_3 + x_2}{2}\right)\frac{x_3 - x_2}{\Delta z} - D\left(\frac{x_1 + x_2}{2}\right)\frac{x_2 - x_1}{\left(\frac{\Delta l + \Delta z}{2}\right)}\right] \tag{15}$$

and

$$Q_i = \frac{1}{\Delta z}\left[D\left(\frac{x_{i+1} + x_i}{2}\right)\frac{x_{i+1} - x_i}{\Delta z} - D\left(\frac{x_i + x_{i-1}}{2}\right)\frac{x_i - x_{i-1}}{\Delta z}\right]; \quad i = 3,4,\ldots \tag{16}$$

It should be pointed out that for $a_1 = 0.5$, Eq. (14) and Eq. (16) are exactly the Crank-Nicholson scheme.

To implement Eqs. (11), (12), (14),(15), and (16) with D given by Eq. (2), the Q_i are linearized with respect to $x_i(t+1)$. This results in the tridiagonal system:

$$R\underline{x}(t+1) = \underline{v} \text{ or } \underline{x}(t+1) = R^{-1}\underline{v} \tag{17}$$

where $\underline{v}$ and the nonzero elements of R are given in Appendix I.

A scheme that propagates as in Eq. (17) would result in an ever increasing top layer thickness Δl, and a resulting loss of accuracy. To avoid this, when Δl surpasses Δz, the top layer is split parallel to the surface into two parts, with the bottom having a thickness of Δz. This layer becomes the new layer 2, increasing the indices of the underlying layers by one (Fig. 4). This algorithm involves no averaging since only layers of thickness Δz are shifted.

It is not practical to have the dimensionality of the vector $\underline{x}$ always increasing. Furthermore, reflectance is effectively a function of the composition of only the top 2000 to 3000Å. For these reasons, whenever a new layer is created by the division of the top layer into two parts, the bottom layer is discarded.

A final issue to be addressed is the boundary condition for the bottom-most layer. Let n denote the index of this layer. Then, in general, the composition of the layer below is not available (with the exception being the occasion when a new layer was created in the previous time step). So a boundary condition is needed for layer n, or equivalently, x_{n+1} must be estimated. Three possible choices were considered.

The first is zero compositional slope, i.e.

$$x_n = x_{n+1} \tag{18}$$

The rationale for this boundary condition is that the composition profile becomes uniform at a large distance from the top due to interdiffusion.

The second candidate for the boundary condition is no net diffusion where

$$D\left(\frac{x_{n+1}+x_n}{2}\right)\frac{x_{n+1}-x_n}{\Delta z} = D\left(\frac{x_n+x_{n-1}}{2}\right)\frac{x_n-x_{n-1}}{\Delta z} \tag{19}$$

The rationale is that sufficient time has elapsed since the nth layer was grown so that x_n has approached its steady-state value

The third candidate for the boundary condition is constant compositional slope, i.e.

$$x_{n+1} - x_n = x_n - x_{n-1}. \tag{20}$$

The impact of these conditions on the IMP model (17) is given in Appendix II.

If the actual slope at the nth layer is zero, as is the case at the beginning of interdiffused multilayer process growth on a CdTe substrate when the nth layer is deep in the substrate, then all of the above truncation schemes are exact. For example, after one typical IMP cycle, 1300Å of alloy have been deposited with an accompanying 250–300Å erosion of the CdTe substrate due to diffusion. The model with Δz = 50Å and n = 50 has its nth layer in the substrate, a region of zero slope and x = 1.

Figure 5 compares the composition profile after one IMP cycle for the model with n = 50 (solid line), which has no truncation error, with the profile with n = 30 using the three truncation schemes. The first scheme is represented by the plusses, the second by the dashes, and the third by the dots. Errors are only evident after the 26th layer (60075Å) with the second and third schemes giving very good results.

The model, Eq. (17), using boundary condition (19) gives no stability problems for a_1 = 1 (fully implicit) and allows a Δz of 50Å with Δt = 0.2 s and a_1 = 0.5 (Crank-Nicholson).

MODELING OF GROWTH RATE

The previous development does not address modeling of the growth rate g(t) that affects the top layer [see Eq. (11)]. A typical IMP cycle consists of, in order, a HgTe growth phase, a HgTe flush phase, a CdTe growth phase, and a CdTe flush phase. During a HgTe

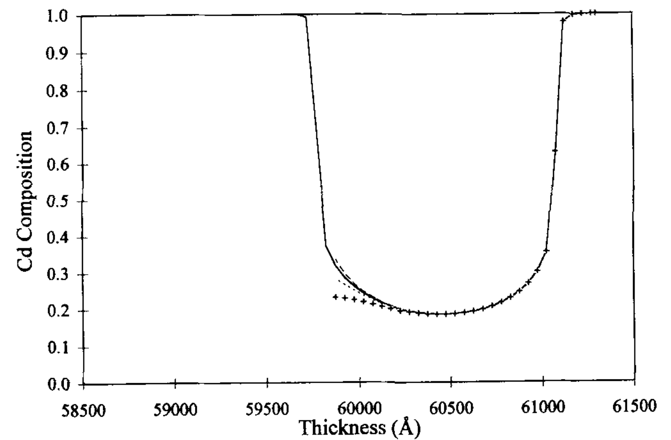

Fig. 5. Composition profiles after one IMP growth cycle on CdTe. The solid line represents no truncation error; the pluses, the zero slope truncation method; the dashed line, the no diffusion method; and the dotted line, the constant slope method. The CdTe substrate surface was located at 60000Å, and Δt was 0.5 s.

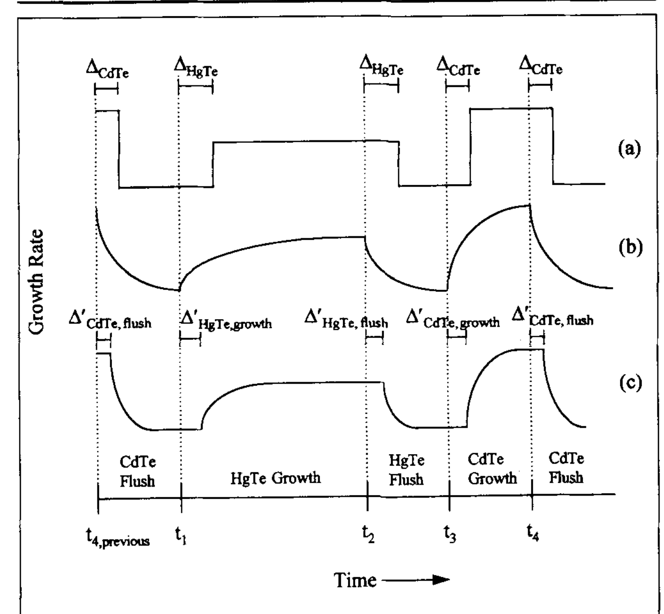

Fig. 6. Schematic of the growth rate modeling scheme. The growth rates are shown when modeling precursor dilution as (a) plug flow, (b) a perfectly mixed tank, and (c) the intermediate case used here.

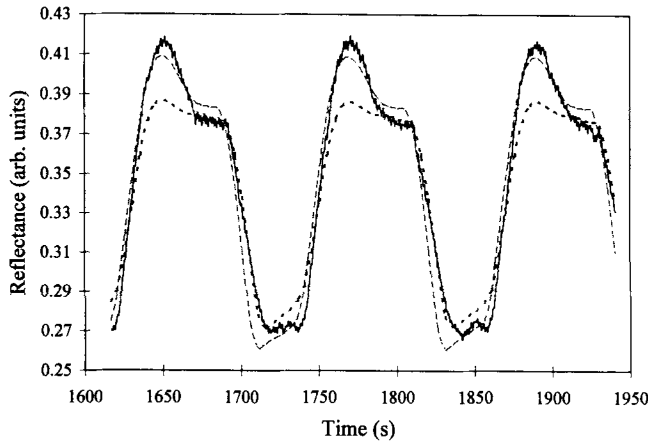

Fig. 7. Measured (solid line) and theoretical reflectance output from part of an IMP growth period using Tang and Stevenson diffusion parameters (dotted line) and Zanio and Massopust parameters (dashed line).

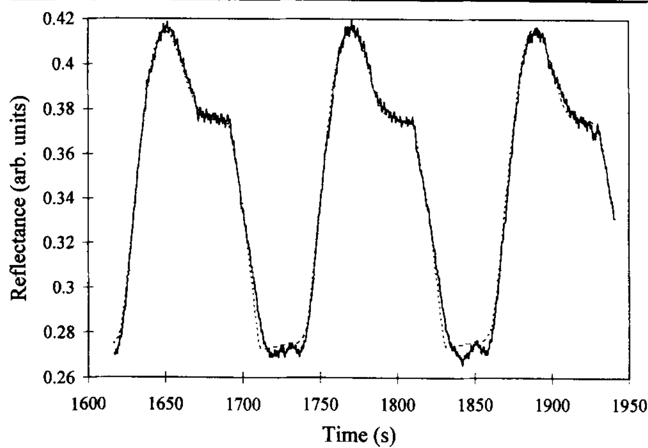

Fig. 8. Measured (solid line) and theoretical (dotted line) reflectance output from part of an interdiffused multilayer process growth period using fitted parameter values.

growth phase, mercury vapor and diisopropyl telluride (DiPTe) are the precursors. In the subsequent flush phase, the flow of DiPTe is halted and the growth rate decays toward zero. In the CdTe growth phase dimethyl cadmium (DMCd) and DiPTe are fed in as precursors. The flow of these precursors is stopped in the ensuing CdTe flush phase, and again growth rate decays to zero.

There are two extreme conditions for modeling the changes in growth rate as the phases are switched. The first is plug flow of the precursors (Fig. 6a), in which case growth rate is zero at the beginning of a HgTe growth phase until the time required to transport the precursors, Δ_{HgTe}, elapses and then g(t) steps up to a constant value, g_{HgTe}. In the following flush phase, the growth rate steps down to zero, but only after Δ_{HgTe} has passed. The growth rate for these two phases can be expressed as

$$g(t) = \begin{cases} 0, & t_1 < t \le t_1 + \Delta_{HgTe} \\ g_{HgTe}, & t_1 + \Delta_{HgTe} < t \le t_2 + \Delta_{HgTe} \\ 0, & t > t_2 + \Delta_{HgTe} \end{cases} \quad (21)$$

where t_1 denotes the time at the start of the HgTe growth phase and t_2 the time at the start of the flush phase.

The growth rate during the CdTe growth and flush phases follows a similar pattern. It steps up to g_{CdTe} after a transportation lag Δ_{CdTe} has passed in the growth phase and steps down to zero after an interval Δ_{CdTe} in the following flush phase.

The second extreme condition is a perfectly mixed tank which results in immediate concentration changes at the beginning of each phase according to exponential functions (Fig. 6b). At the beginning of the HgTe growth phase, the growth rate increases according to

$$g(t) = g_{HgTe,max}\left[1 - \exp\left(-\frac{t - t_1}{\theta_{HgTe\ growth}}\right)\right],\ t_1 < t \le t_2 \quad (22)$$

where $\theta_{HgTe\ growth}$ is the residence time, or the time constant, of the tank. The growth rate follows Eq. (22) until the HgTe flush phase where g(t) starts decreasing with

$$g(t) = g(t_2)\exp\left(-\frac{t - t_2}{\theta_{HgTe\ flush}}\right),\ t_2 < t \le t_3 \quad (23)$$

This growth rate condition holds until the start of the CdTe growth phase in which g(t) increases according to an expression similar to Eq. (22). The growth rate then decreases during the CdTe flush phase following an expression similar to Eq. (23).

In reality, precursor concentration, and therefore growth rate, varies according to conditions intermediate to the above two extremes. This intermediate state is modeled here by combining aspects of the two extreme conditions. Consider the following expression for growth rate:

$$g(t) = \begin{cases} 0, & t \le t_1 + \Delta'_{HgTe growth} \\ g_{HgTe}\left[1 - \exp\left(-\frac{t - (t_1 + \Delta'_{HgTe\ growth})}{\theta'_{HgTe\ growth}}\right)\right], & \\ & t_1 + \Delta'_{HgTe growth} < t \le t_2 + \Delta'_{HgTe flush} \end{cases} \quad (24)$$

which results from integrating a first order plus time delay model.

Both extreme models [Eqs. (21), (22), and (23)] can be viewed as special case of Eq. (24). The plug flow case is obtained for values $\Delta'_{HgTe\ growth} = \Delta_{HgTe}$ and $\theta'_{HgTe\ growth} = 0$, while the perfectly mixed tank case is obtained for $\Delta'_{HgTe\ growth} = 0$ and $\theta'_{HgTe\ growth} = \theta_{HgTe\ growth}$. Thus, an intermediate state can be modeled using

$$0 < \Delta'_{HgTe\ growth} < \Delta_{HgTe}$$
$$0 < \theta'_{HgTe\ growth} < \theta_{HgTe\ growth}$$

Modeling all phases in similar manner gives the following expression for growth rate:

$$g(t) = g(t)$$

$$\begin{cases} g_{HgTe}\left[1-\exp\left(-\frac{t-(t_1+\Delta'_{HgTe\,growth})}{\theta'_{HgTe\,growth}}\right)\right], & t_1+\Delta'_{HgTe\,growth} < t \le t_2+\Delta'_{HgTe\,flush} \\ g_{HgTe}\left[\exp\left(-\frac{t-(t_2+\Delta'_{HgTe\,flush})}{\theta'_{HgTe\,flush}}\right)\right], & t_2+\Delta'_{HgTe\,flush} < t \le t_3+\Delta'_{CdTe\,growth} \\ g_{CdTe}\left[1-\exp\left(-\frac{t-(t_3+\Delta'_{CdTe\,growth})}{\theta'_{CdTe\,growth}}\right)\right], & t_3+\Delta'_{CdTe\,flush} < t \le t_4+\Delta'_{CdTe\,flush} \\ g_{CdTe}\left[\exp\left(\frac{t-(t_4+\Delta'_{CdTe\,flush})}{\theta'_{CdTe\,flush}}\right)\right], & t_4+\Delta'_{CdTe\,flush} < t \le t_{1,next}+\Delta'_{HgTe\,growth} \end{cases} \quad (25)$$

To reduce the number of tunable parameters, the time constants θ' are chosen so that the total deposition equals the deposition obtained in the plug flow case, i.e. equal areas under the two corresponding growth rate curves of Fig. 6. This results in the implicit expression given below for $\theta'_{HgTe\,growth}$ and in similar expressions for the other time constants

$$\Delta_{HgTe} = \Delta'_{HgTe\,growth} + \theta'_{HgTe\,growth} \cdot \left[1-\exp\left(-\frac{(t_2+\Delta'_{HgTe\,flush})-(t_1+\Delta'_{HgTe\,growth})}{\theta'_{HgTe\,growth}}\right)\right] \quad (26)$$

To further reduce the number of tunable parameters, we assume that the ratio of a delay Δ' to the corresponding delay Δ in the plug flow model is independent of the material being deposited, in which case the tunable parameters in the growth model reduce to the transportation lag fractions:

$$\alpha_{growth} = \frac{\Delta'_{CdTe\,growth}}{\Delta_{CdTe}} = \frac{\Delta'_{HgTe\,growth}}{\Delta_{HgTe}} \quad (27)$$

and

$$\alpha_{flush} = \frac{\Delta'_{CdTe\,flush}}{\Delta_{CdTe}} = \frac{\Delta'_{HgTe\,flush}}{\Delta_{HgTe}} \quad (28)$$

EXPERIMENTAL DETAILS

The diffusion and growth model was tested using laser reflectometry measurements of IMP growth of MCT. The material was grown in a horizontal rectangular duct silica reactor at atmospheric pressure. A 2 cm diameter optical window was mounted in a turret approximately 3 cm above the top reactor wall. The window was flushed with helium gas and no deposition on the window was observed during growth. A chopped beam from a 2 mW high stability HeNe laser operating a 6328Å was directed at a near normal incidence angle onto the wafer, and the intensity of the reflected light was measured by a silicon detector. A schematic diagram of the experimental setup can be found in Bajaj et al.[3]

The IMP experimental run used to test the model was done at 380°C using a pyrolytic boron nitride heater and started with a 60.8 s HgTe growth phase. During this phase, the blanket flow rate was 5 L/min. The Hg vapor came from a liquid-Hg-filled boat placed at the entrance zone of the reactor and heated to 210°C. The Hg growth phase was followed by a 20 s HgTe flush phase in which the blanket flow rate was ramped to 8 L/min. During these first two phases, 936Å of HgTe were deposited. Next, without altering the blanket flow rate, a 19 s CdTe growth phase was initiated. A 20 s CdTe flush phase followed where the blanket flow rate was ramped down to 5 L/min. During these last two phases, 276Å of CdTe were deposited. The total cycle period, then, was 119.8 s.

The IMP run was designed to give a homogenized alloy composition of x = 0.23, corresponding to a longwave infrared absorber layer. This final composition was confirmed by ex situ infrared transmission measurements.

COMPARISON WITH EXPERIMENTAL RESULTS

The process was modeled using Eq. (24) and the equations given in Appendices I and II. To simplify modeling, changes in the blanket flow rate were treated as steps occurring at the start of deposition in the two growth phases. This results in plug flow delays of Δ_{HgTe} = 10.8 s and Δ_{CdTe} = 6.3 s.

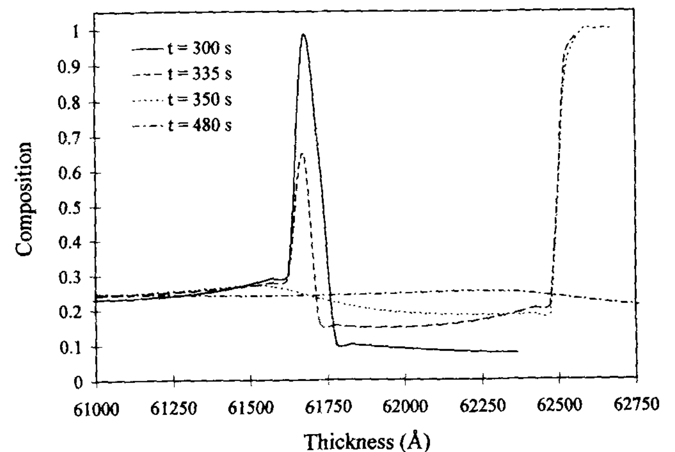

Fig. 9. Composition profile vs thickness as a function of time for a portion of an IMP growth run. The solid line represents the profile 300 s into the growth run, the dashed line at 335 s, the dotted at 350 s, and the dot-dashed at 480 s.

Reflectance was calculated from theoretical expressions that give the reflectance intensity from a stack of thin films with abrupt interfaces and varying optical indices.[3,22,23] The reflectance expression used can be found in Bajaj et al.[3] The complex refractive index of each layer of the MCT alloy was calculated using the average of the complex refractive indices of HgTe and CdTe, weighted by the mole fraction of the individual components.

Parameters were initially set to values which were reported in literature or based on best engineering estimates. The complex refractive indices for CdTe and HgTe were initially set to

$$N_{CdTe} = 3.04 - i\,0.253 \quad (29)$$
$$N_{HgTe} = 3.93 - i\,1.19 \quad (30)$$

which were based on ellipsometry measurements by Rhiger.[24] The transportation lag fractions were initially set at the intermediate value $\alpha_{growth} = \alpha_{flush} = 0.5$. For the diffusion parameters, the Tang and Stevenson[11,12] expression gives at 380°C $A = 1.56 \cdot 10^{-4}$ $\mu m^2/s$ and $B = 9.06$, while the Zanio and Massopust[13] expression gives $A = 4.02 \cdot 10^{-5}$ $\mu m^2/s$ and $B = 8.13$. It should be noted that these values were from expressions that were obtained by fitting data from higher temperatures.

Figure 7 compares the experimental reflectance profile (solid line) with the predicted profiles obtained using the Tang and Stevenson[11,12] diffusion parameters (dotted line) and the Zanio and Massopust[13] parameters (dashed line). The figure shows that the model with the Zanio and Massopust[13] parameters agrees fairly well with the experimental data. The model with the Tang and Stevenson[11,12] parameters predicts very poorly the extrema but predicts well the intermediate regions. The significant difference in model behavior show that the model is quite sensitive to the diffusion parameters.

With parameter fitting, the agreement of the model with the measurements can be improved considerably. Parameters fitted, in addition to the diffusion parameters, were the transportation lag fractions (α_{growth} and α_{flush}), and the complex refractive index N_{HgTe}. The latter was fitted because somewhat different values have been reported.[3,24] The curvature of the reflectance curve from the HgTe growth phase of the first IMP cycle is mostly dependent on α_{growth}. Fitting α_{growth} using this first growth phase gave $\alpha_{growth} = 0.61$. The remaining five parameters were fitted using a Levenberg-Marquardt method[25] of nonlinear least squares optimization resulting in the following values:

$$A = 1.14 \times 10^{-3}\ \mu m^2/s$$
$$B = 16.90$$
$$N_{HgTe} = 4.01 - i\,1.18$$
$$\alpha_{flush} = 0.54$$

The reflectance from the model with the fitted parameters is compared to measured output in Fig. 8. Very good agreement is observed. It is noteworthy that the values for the complex refractive index of HgTe are close to the default values in Eq. (30).

DISCUSSION

The fitting of the dynamic interdiffusion model to the reflectance data in Fig. 8 enables new insights to the dynamics of the IMP. The relaxation of the compositional profile cannot be deciphered from ex situ characterization because the compositional profile is by then fully interdiffused. The dynamics of interdiffusion are important when considering the possibility of introducing misfit dislocations due to the 0.3% lattice mismatch between CdTe and HgTe. The time evolution of the composition profiles, shown in Fig. 9, was obtained using the fitted diffusion and growth parameters given above. During the HgTe growth phase, the compositional profiles show that the interdiffusion is so rapid that the surface composition never reaches that of the binary. This is a significant factor in the relaxation of the lattice and is a consequence of the larger diffusion coefficient at the HgTe end of the pseudobinary. By contrast, the much thinner CdTe layers do achieve a binary composition but rapidly erode as Cd diffuses into the surrounding Hg rich alloy. Interdiffusion becomes even more rapid as the Cd composition of the peak decreases, resulting in a largely homogeneous alloy composition within 180 s of deposition. This is consistent with ex situ characterization such as Rutherford backscattering which shows no residual compositional modulation for normal IMP period thicknesses and compositions.[26]

CONCLUDING REMARKS

A dynamic model was developed for the interdiffused multilayer process which has enabled, for the first time, insight to the interdiffusion process in the $Hg_{1-x}Cd_xTe$ system during IMP growth and has important consequences for the optimization of growth conditions to avoid inhomogeneities and strain induced defects. These features are critical for the application of this material to longwave infrared detection. Other possible uses of the model include: screening of feedback control methods, development of state estimators which can then be used for controller design, and the development of model predictive control laws. It is anticipated that this model would also be applicable to the interpretation of in situ reflectometry of other material systems where interdiffusion is a significant parameter.

ACKNOWLEDGMENT

The authors at the University of Florida gratefully acknowledge the support of Rockwell International Corporation.

REFERENCES

1. J. Turnicliffe, S.J.C. Irvine, O.D. Dosser and J.B. Mullin, *J. Cryst. Growth* 13, 245 (1984).
2. J.B. Mullin, J. Geiss, S.J.C. Irvine, J.S.Gough and A. Royale, *Mater. Res. Soc. Symp. Proc.* 90, 367 (Pittsburgh, PA: Mater. Res. Soc., 1987).
3. J. Bajaj, S.J.C. Irvine, H.O. Sankur and S.A. Svoronos, *J. Electron. Mater.* 22, 899 (1993).

4. S.J.C. Irvine, J. Bajaj and H.O. Sankur, *J. Cryst. Growth* 21, 654 (1992).
5. S.J.C. Irvine, E.R. Gertner, L.O. Bubulac, R.V. Gil and D.D. Edwall, *Semicond. Sci. Technol.* 6, C15 (1991).
6. M.-F.S. Tang and D.A. Stevenson, *J. Vac. Sci. Technol. A* 6, 2650 (1988).
7. M.-F.S. Tang and D.A. Stevenson, *J. Vac. Sci. Technol. A* 7, 2650 (1989).
8. C.G. Morgan-Pond, *J. Electron. Mater.* 20, 399 (1991).
9. Y. Jianrong, Y. Zhenzhong, L. Jiming and T. Dingyuan, *J. Cryst. Growth* 114, 351 (1991).
10. Y. Kim, A. Ourmazd and R.D. Feldman, *J. Vac. Sci. Technol. A* 8, 1116 (1990).
11. M.-F.S. Tang and D.A. Stevenson, *J. Vac. Sci. Technol.* A 5, 3124 (1987).
12. M.-F.S. Tang and D.A. Stevenson, *Appl. Phys. Lett.* 50, 1272 (1987).
13. K. Zanio and T. Massopust, *J. Electron. Mater.* 15, 103 (1986).
14. K. Zanio, *J. Vac. Sci. Technol. A* 4, 2106 (1986).
15. B.W. Ludington, *Mater. Res. Soc. Symp. Proc.* 90, 437 (Pittsburgh, PA: Mater. Res. Soc., 1987).
16. C.J. Rossouw, G.N. Pain, S.R. Glanville and D.C. MacDonald, *J. Cryst. Growth* 106, 673 (1990).
17. D.K. Arch, J.P. Faurie, J.-L. Staudenmann, M. Hibbs-Brenner and P. Chow, *J. Vac. Sci. Technol. A* 4, 2101 (1986).
18. K. Zanio and K. Hay, *Mater. Res. Soc. Symp. Proc.* 90, 39 (Pittsburgh, PA: Mater. Res. Soc., 1987).
19. J.G. Heming and D.A. Stevenson, *J. Cryst. Growth* 82, 621 (1987).
20. N. Archer and H. Palfrey, *J. Electron. Mater.* 20, 419 (1991).
21. W.H. Press, B.P. Flannery, S.A. Teukolsky and W.T. Vetterling, *The Art of Scientific Computing*, (Cambridge: Cambridge University Press, 1988).
22. W. Southwell, personal communication.
23. H.A. Macleod, *Thin-Film Optical Filters*, 2nd Ed., (New York: Macmillan Publishing Company, 1986).
24. D. Rhiger, *J. Electron. Mater.* 22, 887 (1993).
25. T.R. Cuthbert, *Optimization Using Personal Computers with Applications to Electrical Networks*, (New York: John Wiley & Sons, Inc., 1987).
26. A.J. Avery, D.J. Diskett, D.W. Lane, J. Giess and S.J.C. Irvine, *Nucl. Instr. Meth. Phys. Res.* B45, 181 (1990).

APPENDIX I

The IMP Model

The discretization and linearization of the growth and diffusion equations result in a tridiagonal system of equations of the form

$$R\underline{x}(t+1) = \underline{v} \text{ or } \underline{x}(t+1) = R^{-1}\underline{v} \tag{A1.1}$$

where the nonzero components of R are

$$R_{11} = 1 + a_1\Delta t\frac{g(t+\Delta t)}{\Delta l(t+\Delta t)} + \frac{2a_1\Delta t}{\Delta l(t+\Delta t)(\Delta l(t+\Delta t)+\Delta z)}D\left(\frac{x_1(t)+x_2(t)}{2}\right)\left(1+\frac{B}{2}(x_2(t)-x_1(t))\right) \tag{A1.2}$$

$$R_{12} = -\frac{2a_1\Delta t}{\Delta l(t+\Delta t)(\Delta l(t+\Delta t)+\Delta z)}D\left(\frac{x_1(t)+x_2(t)}{2}\right)\left(1-\frac{B}{2}(x_2(t)-x_1(t))\right) \tag{A1.3}$$

$$R_{21} = -\frac{2a_1\Delta t}{\Delta z(\Delta l(t+\Delta t)+\Delta z)}D\left(\frac{x_1(t)+x_2(t)}{2}\right)\left(1+\frac{B}{2}(x_2(t)-x_1(t))\right) \tag{A1.4}$$

$$R_{22} = 1 + \frac{2a_1\Delta t}{\Delta z(\Delta l(t+\Delta t)+\Delta z)}D\left(\frac{x_1(t)+x_2(t)}{2}\right)\left(1-\frac{B}{2}(x_2(t)-x_1(t))\right) + \frac{a_1\Delta t}{\Delta z^2}D\left(\frac{x_3(t)+x_2(t)}{2}\right)\left(1+\frac{B}{2}(x_3(t)-x_2(t))\right) \tag{A1.5}$$

$$R_{i,i+1} = -\frac{a_1\Delta t}{\Delta z^2}D\left(\frac{x_{i+1}(t)+x_i(t)}{2}\right)\left(1-\frac{B}{2}(x_{i+1}(t)-x_i(t))\right);\ \text{for } i = 2,3\ldots \tag{A1.6}$$

$$R_{i,i-1} = -\frac{a_1\Delta t}{\Delta z^2}D\left(\frac{x_i(t)+x_{i-1}(t)}{2}\right)\left(1+\frac{B}{2}(x_i(t)-x_{i-1}(t))\right);\ \text{for } i = 3,4\ldots \tag{A1.7}$$

$$R_{ii} = 1 + \frac{a_1\Delta t}{\Delta z^2}D\left(\frac{x_i(t)+x_{i-1}(t)}{2}\right)\left(1-\frac{B}{2}(x_i(t)-x_{i-1}(t))\right) + D\left(\frac{x_i(t)+x_{i+1}(t)}{2}\right)\left(1+\frac{B}{2}(x_{i+1}(t)-x_i(t))\right);\ \text{for } i = 3,4\ldots \tag{A1.8}$$